Part B: Discrete Models

An Inverted Pendulum

Consider the simple hinged cantilever shown below.

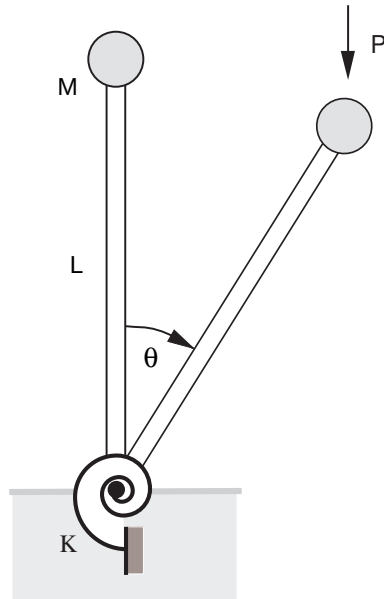

A simple hinged-bar (the inverted pendulum model).

The angle of rotation θ thus describes the location of the mass at any given instant of time. Typically, the vertical force is simply $P = Mg$, but here we assume that an axial load of magnitude P acts independently of the constant mass M.

The energy contributions are

$$V = U + V_P = \frac{1}{2}K\theta^2 - PL(1 - \cos\theta). \tag{1}$$

Similarly the kinetic energy, T, is given by

$$T = \frac{1}{2}ML^2\dot{\theta}^2, \tag{2}$$

and placing these into Lagrange's equations we obtain

$$ML^2\ddot{\theta} + K\theta - PL\sin\theta = 0, \tag{3}$$

and using $\sin\theta = \theta$ for small θ we see an effective natural frequency $\omega^2 = K/(ML^2) - P/(ML)$. Equation (3) can be nondimensionalized by assuming

$$\omega_n^2 = K/ML^2, \qquad p = PL/K, \tag{4}$$

to give

$$\ddot{\theta} + \omega_n^2(\theta - p\sin\theta) = 0. \tag{5}$$

Equation (5) is a nonlinear second-order, homogeneous, ordinary differential equation with constant coefficients.

The underlying equilibrium behavior is governed by:

$$\omega_n^2(\theta - p\sin\theta) = 0. \tag{6}$$

This is the first variation of the potential energy and could have been obtained from a direct application of the principle of stationary potential energy. Clearly we have the trivial (or fundamental) equilibrium state for the perfectly upright position $\theta = 0$. However, we see another (post-buckled) solution to equation (6) is (for $p > 1$)

$$p = \frac{\theta}{\sin\theta}. \tag{7}$$

Equation (7) is plotted together with the trivial solution in part (a).

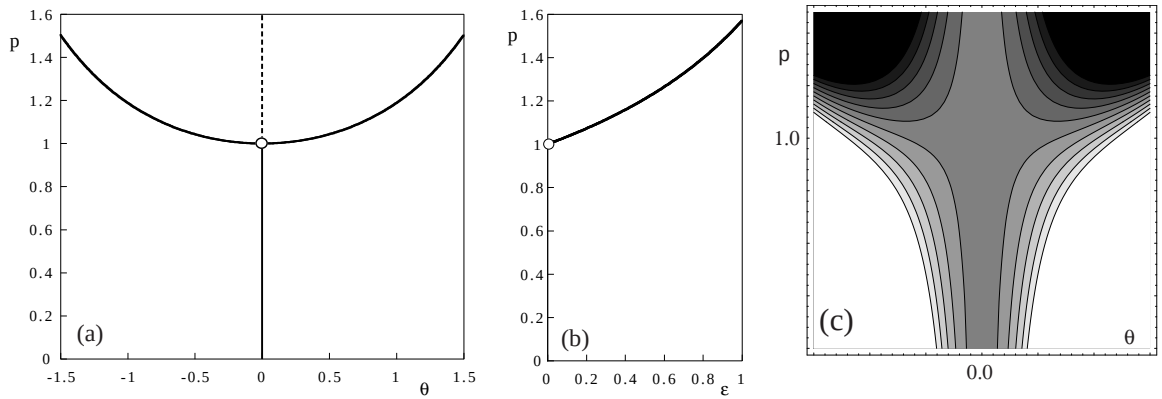

The inverted pendulum, (a) and (b) Equilibrium paths; (c) potential energy contours (truncated for extreme levels).

These paths intersect at $p = 1$, i.e., $P = K/L$. This is the critical load of the structure at which point the trivial equilibrium position gives way to an inclined position. That the trivial equilibrium path is unstable for loads greater than $p = 1$ is established by examining the curvature of the total potential energy in the vicinity of equilibrium. For stability it is sufficient that

$$\frac{d^2V}{d\theta^2} > 0, \tag{8}$$

and thus for $\theta = 0$ the above condition is only satisfied if $p < 1$.
In order to test the stability of the secondary (post-buckled) solution we evaluate equation (8) for the system along the secondary path described by equation (7), which results in

$$\frac{d^2V}{d\theta^2} = 1 - p\cos\theta. \tag{9}$$

This is clearly positive (and indicative of stability) provided

$$p < \frac{1}{\cos\theta}. \tag{10}$$

Therefore, for physically reasonable deflections, i.e., $\theta < \pi/2$, the post-critical equilibrium paths are stable since placing equation (7) into equation (10) leads to

$$1 - \theta \cot \theta < 0. \tag{11}$$

Supposing the end load was gradually increased, we would follow the y-axis with no deflection until the critical value was reached, at which point (and under further increase in P), the system would rotate either in the positive or negative direction. We recognize this type of stable-symmetric bifurcation as a super-critical pitchfork bifurcation.

In a practical situation we would expect the system to have a preferred direction of deformation: it is unreasonable to expect the system to be perfectly vertical at initial equilibrium. Indeed, our earlier experience of symmetric branching behavior highlighted the importance of breaking the symmetry in order to generate generic results. Thus, a small bias or geometric imperfection is built in to the model by assuming the torsional spring is unstressed when $\theta = \theta_0$ (rather than when $\theta = 0$). This changes the total potential energy expression to

$$V = \frac{1}{2}K(\theta - \theta_0)^2 - PL(\cos\theta_0 - \cos\theta), \tag{12}$$

where we still use $\theta = 0$ as the origin, and a corresponding equilibrium condition

$$\frac{dV}{d\theta} = (\theta - \theta_0) - p\sin\theta = 0, \tag{13}$$

where V is now in nondimensional form, which can be rearranged to give

$$p = \frac{(\theta - \theta_0)}{\sin\theta}. \tag{14}$$

Stability is obtained from

$$\frac{d^2V}{d\theta^2} = 1 - p\cos\theta, \tag{15}$$

which when evaluated on the primary (i.e., from zero load) equilibrium curve indicate stability (since $p < 1/(\cos\theta_e)$). In part (a) of the figure they are identified by different dashed lines for different initial imperfections. In part (b) we can follow the local minima of the potential energy (at fixed load levels).

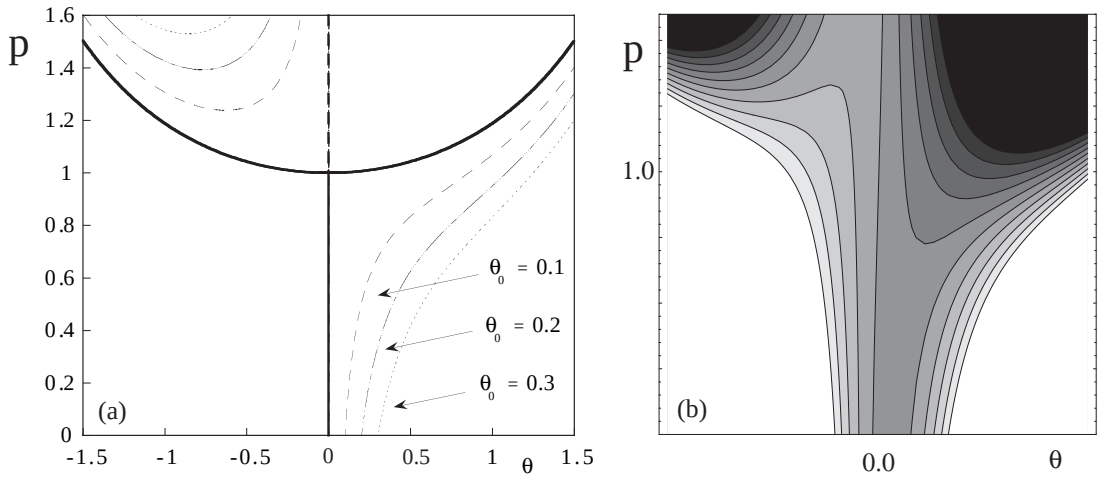

(a) The equilibrium paths and (b) potential energy of the imperfect inverted pendulum model (truncated for extreme levels).

Expanding the sine term in equation (5) about zero and dropping higher order terms leads to

$$\ddot{\theta} + \omega_n^2(1-p)\theta = 0. \tag{16}$$

Here, we are assuming that although the mass provides the axial load the inertia is independent. The linearized (effective) natural frequency drops towards zero as the critical load is approached

$$\omega_n \to 0, p \to 1, \tag{17}$$

and, with Harmonic motion $\theta(t) = c \sin \omega t$, there is a linear relationship between the applied load and the square of the natural frequency $\omega^2 = \omega_n^2(1-p)$ where $p = PL/K$ and $\omega_n^2 = K/ML^2$.

We would expect to have oscillatory behavior about the stable postbuckled paths. We return to equation (5) and expand about a general equilibrium path

$$\theta = \theta_e + \delta. \tag{18}$$

Placing this in equation (5) we have

$$\ddot{\delta} + \omega_n^2[(\theta_e + \delta) - p\sin(\theta_e + \delta)] = 0. \tag{19}$$

Assuming δ is small such that $\cos\delta \approx 1$ and $\sin\delta \approx \delta$, and since $\theta_e - p\sin\theta_e = 0$ we are then left with the linearized (variational) equation of motion

$$\ddot{\delta} + \omega_n^2[1 - p\cos\theta_e]\delta = 0. \tag{20}$$

Linking time and axial load linearly we have

$$\ddot{\theta} + \theta - 0.01\tau \sin\theta = 0, \tag{21}$$

where the critical load is reached after 100 time units have elapsed. We have also scaled the time according to

$$\tau = \omega_n t, \tag{22}$$

and hence the overdot in equation (21) signifies $\dot{\theta} \equiv d\theta/d\tau$. Initial conditions were chosen as $\theta(0) = 0.1, \dot{\theta}(0) = 0.0$ to start not too far away from the equilibrium, and the result of a numerical simulation is shown in the figure below:

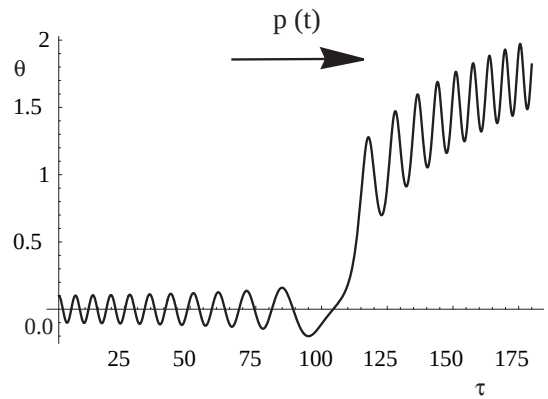

A time series evolving through increasing axial load.

Another conceptual aid in understanding this dynamic behavior is to imagine a small ball rolling on the potential energy surface given by equation (1). For small oscillations (where the linearized equation of motion is appropriate) we see how the evolution of the ball motion in this slowly evolving environment follows the local minima of the underlying potential energy function:

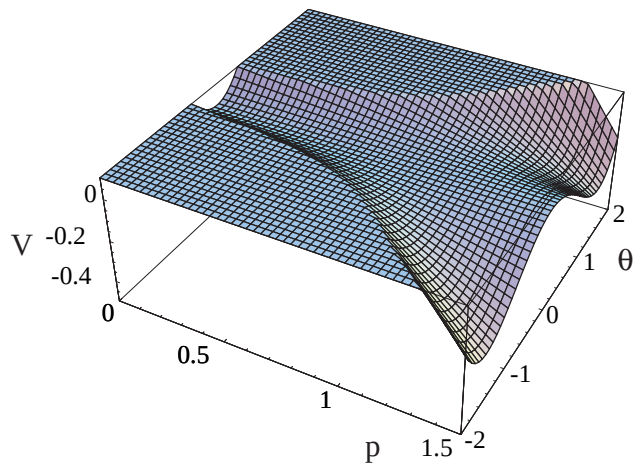

Potential energy surface as a function of axial load.

Plotting contours of constant total energy are shown below for $p = 0.8$ in part (a) and $p = 1.2$ in part (b), with again the darker shades indicating lower levels of total potential energy. When $p = 1.2$ we have symmetric stable equilibria at $\theta_e = \pm 1.027$. The origin is of course a saddle point at this level of load. Initial conditions close to the stable locations would result in approximately linear vibrations according to the solutions of equation (20).

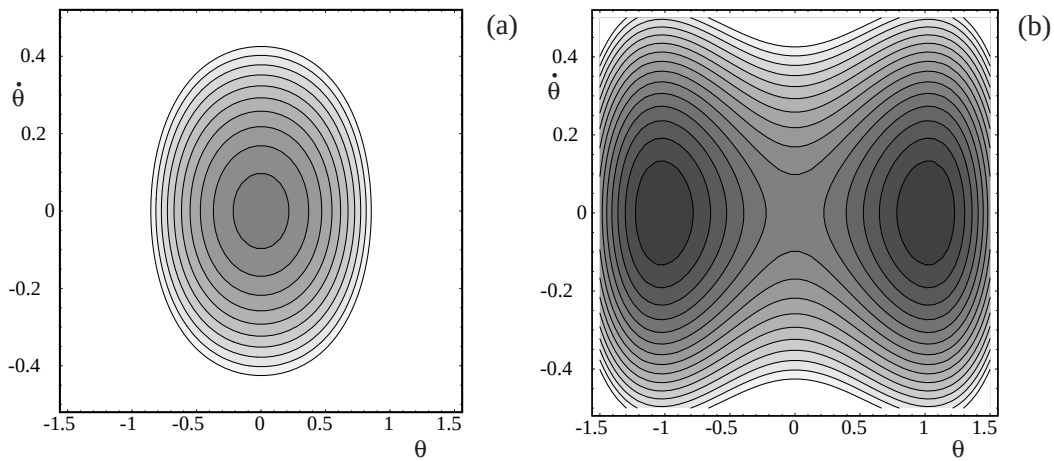

Contours of total energy. (a) p = 0.8, (b) p = 1.2

An example of nonlinear periodic oscillations is shown below. Indeed, for moderately large amplitudes we would find markedly asymmetric oscillations without a traverse of the upright position. A limited amount of analytic progress can be made in such a situation if we retain higher-order terms in the Taylor series expansion about equilibrium. An example of this type of motion (which is very close to the homoclinic solution starting and finishing at the saddle) is shown in part (c) below:

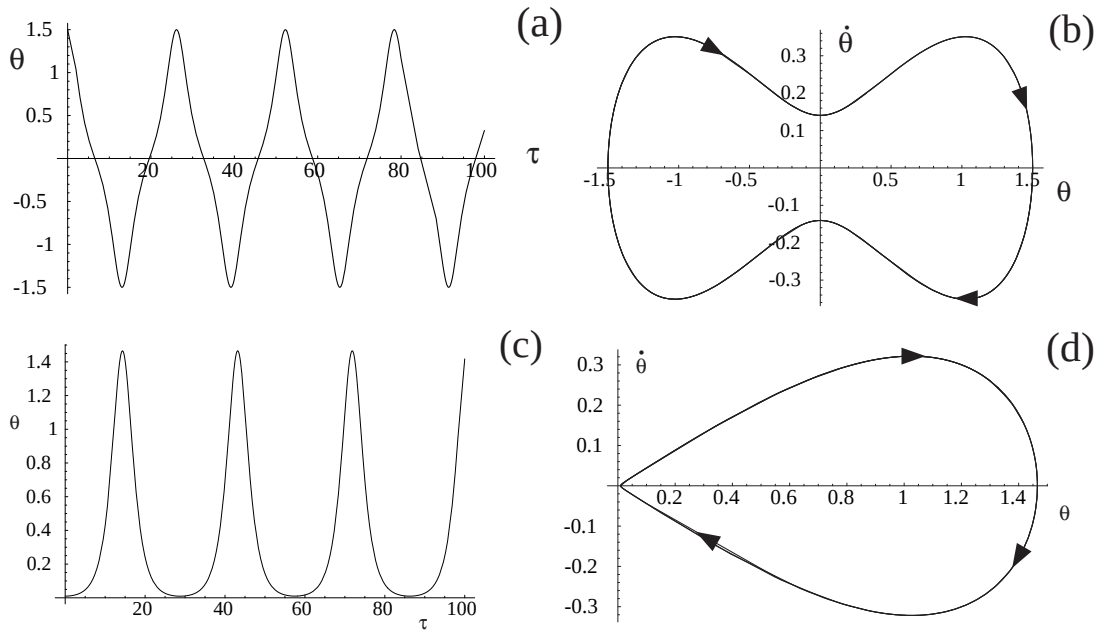

Typical large amplitude oscillations. Both cases correspond to $p = 1.2$*: (a) and (b)* $\theta(0) = 1.5, \dot{\theta}(0) = 0.0$*, (c) and (d)* $\theta(0) = 0.01, \dot{\theta}(0) = 0.0$

The conservation of energy can be obtained directly from equations (1) and (2) or we can alternatively use the simple relation

$$\ddot{\theta} = \dot{\theta}\frac{d\dot{\theta}}{d\theta} \tag{23}$$

in equation (5) to separate variables and obtain the velocity as a function of position

$$\dot{\theta} = \pm\sqrt{C - \theta^2 - 2p\cos\theta}, \tag{24}$$

where the constant C depends on the initial conditions. For example, as shown below in (b) we can use the initial conditions to derive a constant $C = 2.42$, and using equation (24) we can confirm, for example, that as the bar passes through its upright position it will be doing so at a nondimensional velocity of 0.141 in either direction. The phase portrait (a plot of velocity versus position) can thus be viewed as a trajectory following one of these contours of constant total energy.

The (nonlinear) natural frequency of large amplitude vibration can be extracted from the phase trajectories:

$$\int_0^t dt = \int_0^{\theta_{max}} \frac{d\theta}{\sqrt{C - \theta^2 - 2p\cos\theta}}, \tag{25}$$

where the period is equal to four times the time it takes to go from 0 to θ_{max}

$$\tau = 4\int_0^{\theta_{max}} \left[C - \theta^2 - 2p\cos\theta\right]^{-1/2} d\theta. \tag{26}$$

Thus taking the initial conditions (and value of C) corresponding to the trajectory in the previous figure we can evaluate the above integral (numerically) to confirm the (near homoclinic) period of 29.34 units.

A Discrete Strut Model

Consider the strut model shown below. It consists of two rigid (massless) links hinged at their supports and in the center where a concentrated mass M is located. Two linear springs provide a restoring force, one against lateral deflection with modulus K, and the other against rotation with modulus C. An axial load of magnitude P acts at the left hand ends which is unrestrained against horizontal movement. The coordinate Q describes the deflected position of the mass, and we can think of the schematic as providing a plan view, i.e., we assume gravity is already taken into account.

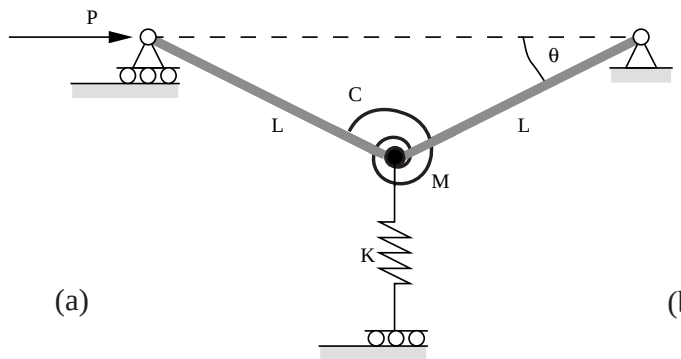

(a)

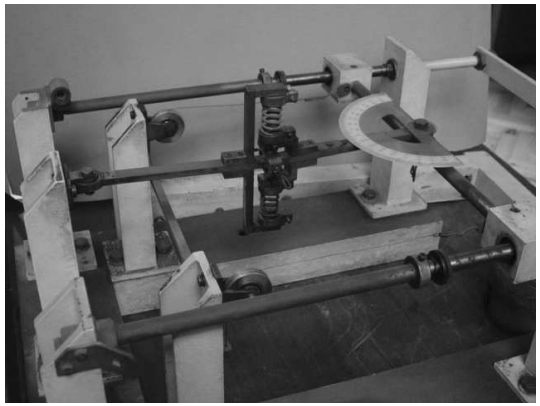

(b)

(a) Schematic of the two-bar link model, (b) Physical realization (UCL).

The total potential and kinetic energies for this system are given by

$$V = 2C\theta^2 + \frac{1}{2}KL^2 \sin^2\theta - 2PL(1 - \cos\theta) \tag{27}$$

and

$$T = \frac{1}{2}ML^2\dot{\theta}^2. \tag{28}$$

Equilibrium solutions are found from

$$\frac{dV}{d\theta} = 4C\theta + KL^2 \sin\theta\cos\theta - 2PL\sin\theta = 0. \tag{29}$$

We immediately see the trivial solution, $\theta_e = 0$, together with the nontrivial solutions given by

$$\Lambda = \alpha\cos\theta + \frac{(1-\alpha)\theta}{\sin\theta} \tag{30}$$

where

$$\Lambda = P/P_{cr}, \quad P_{cr} = \frac{KL^2 + 4C}{2L}, \quad \alpha = \frac{KL^2}{KL^2 + 4C}. \tag{31}$$

The parameter α is a ratio of spring stiffnesses. For example, if $\alpha = 0$ (i.e., K $= 0$) then we have exactly the same type of equilibrium curves as for the model in the previous section. The stability of the equilibrium paths can again be established from the sign of the second derivative of the total potential energy function. However, let us assume initially that $\alpha = 1$ (i.e., C $= 0$) so that we have only a lateral (translational) spring acting. The equilibrium expression simplifies to

$$\Lambda = \cos\theta. \tag{32}$$

In the presence of initial imperfections, the total potential energy becomes

$$V = \frac{1}{2}KL^2(\sin\theta - \sin\theta_0)^2 - 2PL(\cos\theta_0 - \cos\theta) \tag{33}$$

with the first derivative

$$\frac{dV}{d\theta} = KL^2(\sin\theta - \sin\theta_0)\cos\theta - 2PL\sin\theta. \tag{34}$$

Using the nondimensionalization we obtain

$$\Lambda = \frac{(\sin\theta - \sin\theta_0)\cos\theta}{\sin\theta}. \tag{35}$$

In the literature it is sometimes observed that the trigonometric terms are replaced by their series expansion, and retaining the first few terms results in equilibrium paths:

$$\Lambda = \frac{\theta - \theta_0 - \frac{2}{3}\theta^3 + \frac{1}{2}\theta^2\theta_0}{\theta - \frac{1}{6}\theta^3} \approx 1 - \frac{\theta_0}{\theta} + \frac{\theta_0\theta}{3} - \frac{\theta^2}{2} + ..., \tag{36}$$

These non-truncated (equation 35), paths have the form shown below in (a), in which we recognize the characteristic subcritical pitchfork bifurcation.

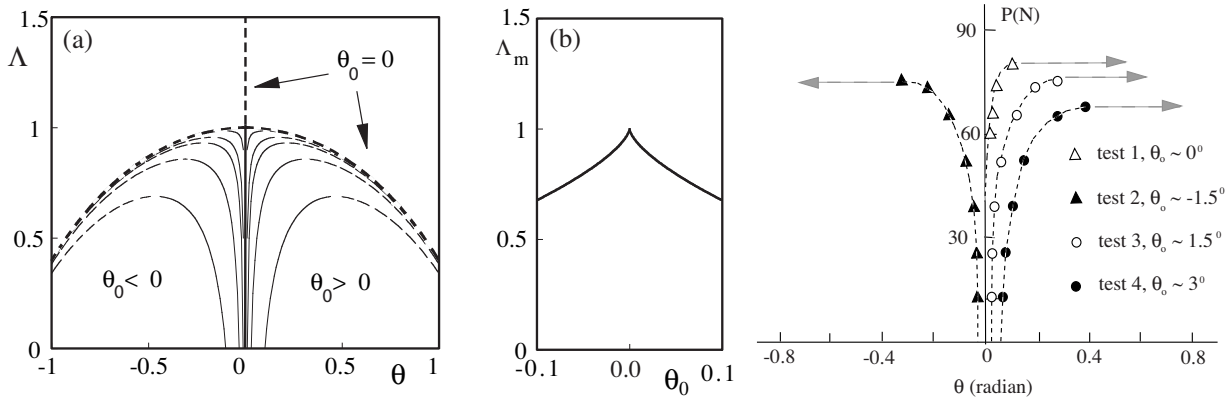

(a) Equilibrium paths for the two-bar link model with a lateral spring and initial geometric imperfections. θ_0 ranges from 0.001 closest to the bifurcation to 0.1, (b) Imperfection sensitivity, (c) measured data (adapted from Croll and Walker).

Complementary paths are also present in this example. However, they prove to be unstable and have little to do with a natural loading path starting near the origin and hence are not included in the plot.

For the imperfect geometry the limit of the stability of the paths coincides with the maximum load Λ_m (the horizontal tangency) for a given path. It can be shown that this occurs when $\theta = \theta_0^{1/3}$, and placing this back in equation (36) results in the cusp geometry also shown in the previous figure (part (b)). This displays an important characteristic of some axially loaded structures: the load carrying capacity of the structure is reduced when initial imperfections are present, i.e., it is imperfection sensitive. This type of sub-critical behavior may then be viewed as a potentially dangerous consequence when compared to the super-critical behavior described in the previous section.

We can again show that the frequency of small oscillations can be obtained using Rayleigh's method:

$$\Omega^2 = 1 - \Lambda \cos\theta - \alpha(1 - \cos 2\theta) \tag{37}$$

where ω is the effective natural frequency

$$\Omega = \frac{\omega}{\omega_n}, \tag{38}$$

$$\omega_n^2 = \frac{4C + KL^2}{ML^2}, \tag{39}$$

and again setting $\alpha = 1$, incorporating initial imperfection θ_0, and simplifying we get

$$\Omega^2 = (1 - 2\theta^2 + \theta\theta_0) - \Lambda(1 - \frac{\theta^2}{2}). \tag{40}$$

We can then plot equation (40) incorporating equation (36) for various initial imperfections, and this is shown below for $\theta_0 = 0.001, 0.01$, and 0.1. Thus we see that the often linear relation between the natural frequency squared and the axial load is not true for initially imperfect geometries, and in fact here the natural frequency drops to zero before the critical load is reached.

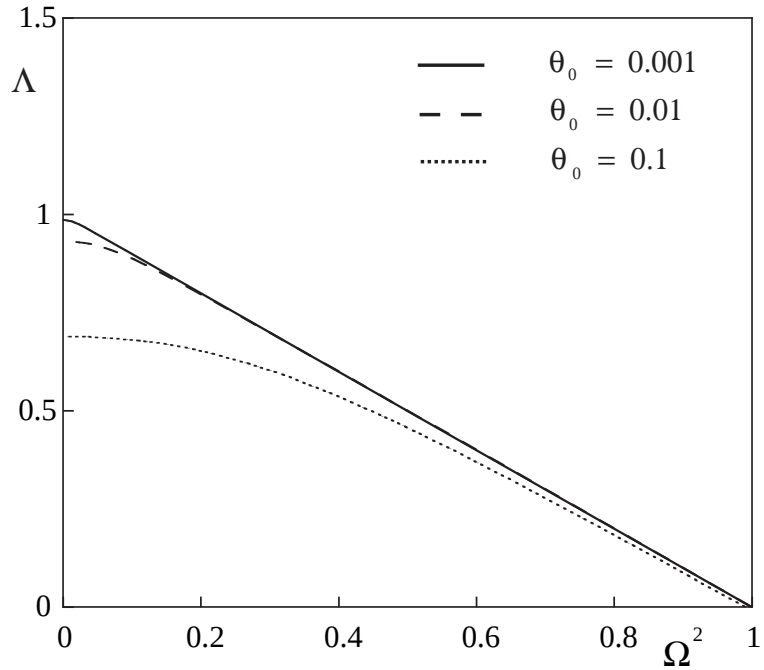

The relation between the natural frequency and axial load for the imperfect unstable symmetric model. $\theta_0 = 0.001, 0.01, 0.1$.

The potential energy surface is plotted as a function of load and deflection below in (a) together with an evolving time series under linearly increasing end load in part (b).

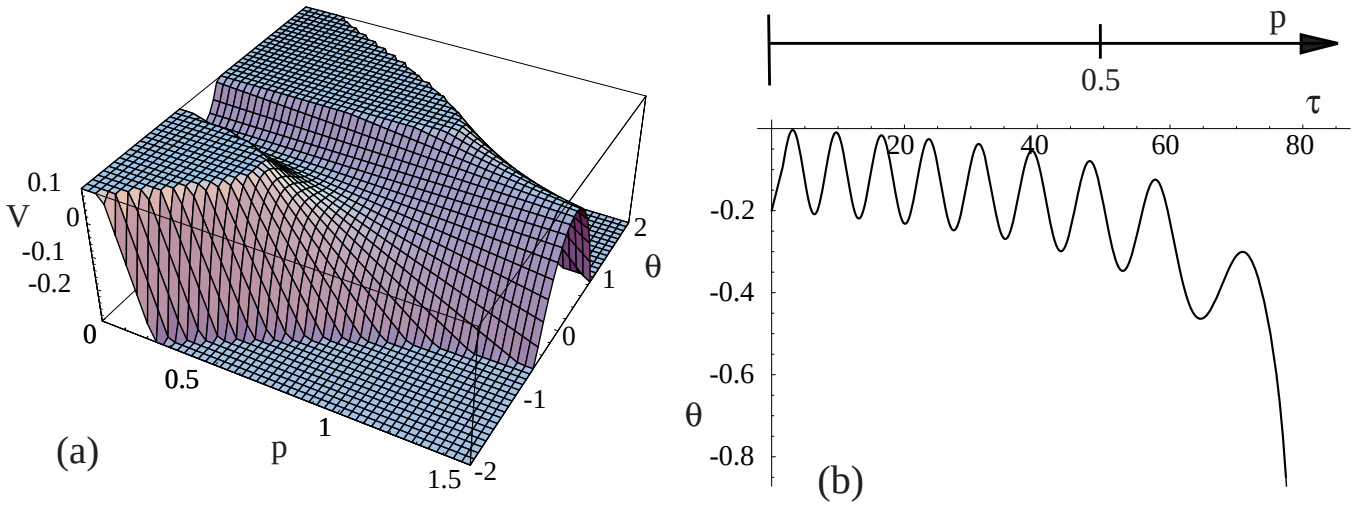

(a) The potential energy surface with an initial imperfection of $\theta_0 = -0.1$. (b) a typical time series evolving through the p-axis, $\theta(0) = -0.2$.

A Three-bar Model

Now let us consider the dynamics and stability of a simple mechanism made up of three rigid links of length L and mass per unit length m. They are hinged at their connections and linear rotational springs of stiffness coefficient k are placed at the two internal joints as shown below:

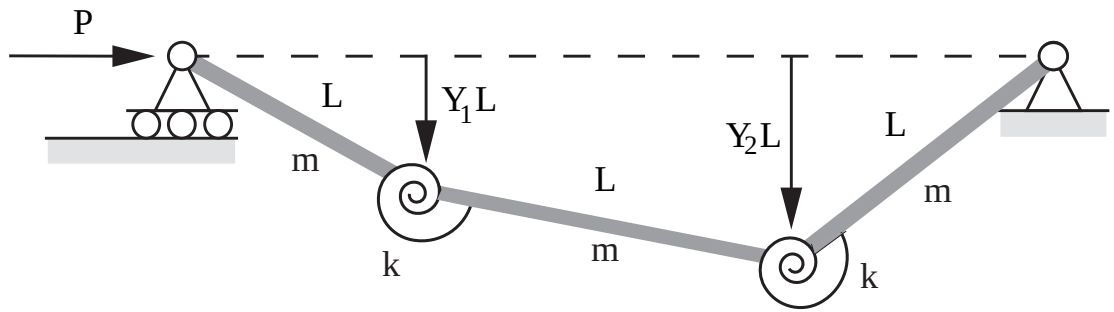

A schematic of a three bar link model (after Thompson and Hunt).

Suppose we choose the lateral deflections as the coordinates (as shown in the figure). In this case we can write down the strain energy stored in the springs as

$$U = \frac{1}{2}k[\sin^{-1} Y_1 - \sin^{-1}(Y_2 - Y_1)]^2 + \frac{1}{2}k[\sin^{-1} Y_2 - \sin^{-1}(Y_2 - Y_1)]^2 \tag{41}$$

which can be expanded to give

$$U = \frac{1}{2}k[5Y_1^2 - 8Y_1Y_2 + 5Y_2^2 + \ldots,]. \tag{42}$$

We can also write down the potential energy associated with the movement of the axial load

$$V = -PL\left[3 - (1 - Y_1^2)^{1/2} - (1 - Y_2^2)^{1/2} - [1 - (Y_2 - Y_1)^2]^{1/2}\right], \tag{43}$$

which can also be expanded to give

$$V = -PL[Y_1^2 - Y_1Y_2 + Y_2^2 + \ldots,]. \tag{44}$$

The kinetic energy for a typical link with displacement a and b at each end is

$$T = \frac{1}{2} m \int_0^L [\dot{a}(1 - x/L) + \dot{b}(x/L)]^2 dx, \tag{45}$$

which, after substitution and adding the effects of all three links leads to

$$T = \frac{1}{2} m L^2 \frac{2}{3} [\dot{Y}_1^2 + \frac{1}{2} \dot{Y}_1 \dot{Y}_2 + \dot{Y}_2^2]. \tag{46}$$

Thus we have our Lagrangian

$$L = T - U + V_P, \tag{47}$$

and a direct application of Lagrange's equation will lead to the equations of motion using the dummy suffix notation

$$T^e_{ij}\,\ddot{Y}_j + V^e_{ij}\,Y_j = 0, \tag{48}$$

and assuming harmonic oscillations $Y_j = A_j \sin \omega t$ obtain

$$V^e_{ij}\,A_j - \omega^2\,T^e_{ij}\,A_j = 0, \tag{49}$$

thus leading to the characteristic equation

$$|V^e_{ij} - \omega^2\,T^e_{ij}| = 0. \tag{50}$$

For the specific case at hand we then have

$$\begin{vmatrix} (5k - 2PL - \omega^2 \frac{2}{3} mL^3) & (-4k + PL - \omega^2 \frac{1}{6} mL^3) \\ (-4k + PL - \omega^2 \frac{1}{6} mL^3) & (5k - 2PL - \omega^2 \frac{2}{3} mL^3) \end{vmatrix} = 0, \quad (51)$$

and using

$$p = \frac{PL}{k} \quad (52)$$

$$\Omega^2 = \frac{\omega^2 mL^3}{k} \quad (53)$$

to get

$$\Omega^2 = \frac{6}{5} \left[(8 - 3p) \pm (2p - 7) \right], \quad (54)$$

and thus the two natural frequencies

$$\Omega_1^2 = \frac{6}{5}(1 - p) \quad (55)$$

$$\Omega_2^2 = 6(3 - p). \quad (56)$$

From equations (55) and (56) we can set the natural frequencies equal to zero to obtain the critical loads

$$p_1 = 1 \quad (P_1 = k/L) \tag{57}$$
$$p_2 = 3 \quad (P_2 = 3k/L). \tag{58}$$

And setting the axial load equal to zero we get the natural frequencies

$$\Omega_1^2 = 6/5 \quad (\omega_1^2 = 6k/(5mL^3)) \tag{59}$$
$$\Omega_2^2 = 18 \quad (\omega_2^2 = 18k/(mL^3)). \tag{60}$$

From equations (55) and (56) we again see the linear relation between the square of the natural frequency and the axial load. The linearity of this relation occurs due to the equivalence of the buckling modes and the natural modes of vibration, having a finite set of generalized coordinates, and the fact that the frequencies depend on a single parameter.

This example can also provide a powerful illustration of the utility of choosing principal coordinates. For this two DOF system it is a simple matter to expand the determinant of equation (51), and of course, there are a myriad of techniques for achieving this numerically for higher-order systems. However, our earlier theory illustrated how coordinate transformations can be useful in the setting up of the equations of motion in going from physical or generalized to principal coordinates. For example:

$$u_1 = \frac{Y_1 + Y_2}{2} \tag{61}$$

$$u_2 = \frac{Y_1 - Y_2}{2} \tag{62}$$

decouples the equations, enabling the critical loads and natural frequencies to be written down immediately. However, this type of direct transformation is usually not obvious *a priori* in a typical analysis. A large variety of numerical algorithms are available to compute this transformation efficiently.

A Snap-through Model

We now consider snap-through buckling associated with a saddle-node bifurcation using the link model shown below.

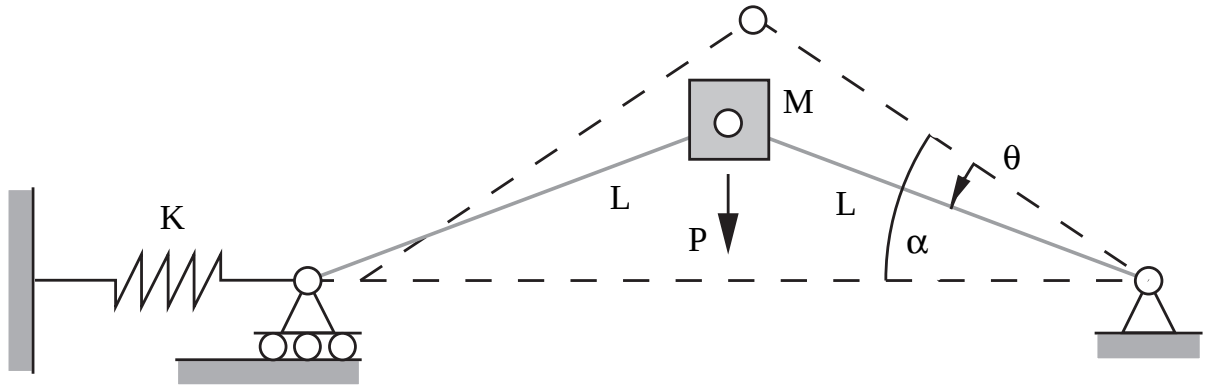

Schematic of a simple arch link model.

The generalized coordinate for this SDOF system is again θ which is measured from the initial rise of the structure (fixed at $\alpha = \pi/8$).

The total potential energy for this model is

$$V = 2KL^2 \left[\cos\left(\alpha - \theta\right) - \cos\alpha\right]^2 - PL\left[\sin\alpha - \sin\left(\alpha - \theta\right)\right] \tag{63}$$

and a kinetic energy of

$$T = \frac{1}{2} ML^2 \dot{\theta}^2. \tag{64}$$

A direct application of Lagrange's equation, and defining

$$p = P/(4KL), \quad \omega_n^2 = 4K/M, \tag{65}$$

leads to the nondimensional equation of motion

$$\ddot{\theta} + \omega_n^2 \left[\cos\left(\alpha - \theta\right) - \cos\alpha\right] \sin\left(\alpha - \theta\right) - p\cos\left(\alpha - \theta\right) = 0. \tag{66}$$

For example a limit point is reached when $p = 0.0116$ which corresponds to a deflection of $\theta = 0.166$ radians, i.e., when the load reaches this value the structure has deflected to nearly 10 degrees and then suddenly snaps through to an inverted position (which is about $\theta = 0.844$ rad, i.e., about 25 degrees below the horizontal).

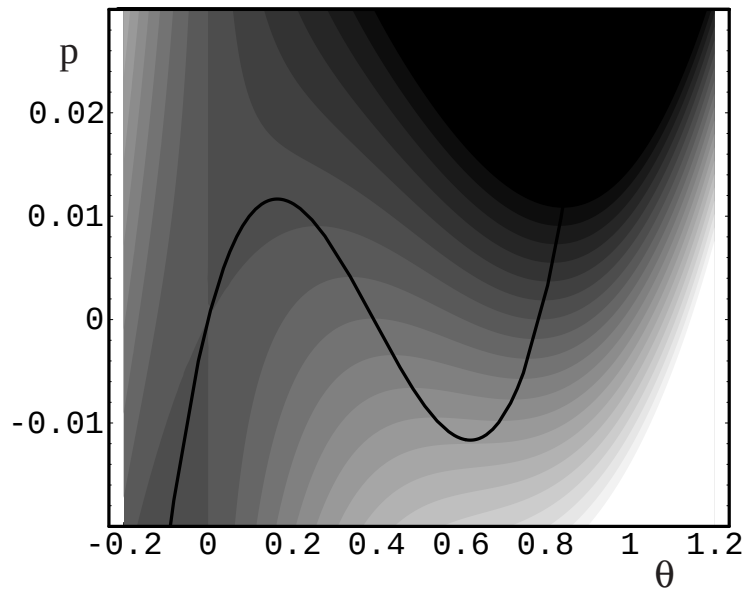

The potential energy surface as a function of axial load with the equilibrium path superimposed.

Conducting a numerical integration we can sweep through the instability using the following loading function

$$p = -0.02 + 0.0001t. \tag{67}$$

An example is shown next, using an initial condition that is 0.01 radians away from stable equilibrium, and $\omega_n = 1$ for convenience. Using the ramp function of equation (67) thus converts to an anticipated critical time of $t_{cr} = 316$. The loss of stability is abrupt (albeit slightly delayed) under the gradual increase in load.

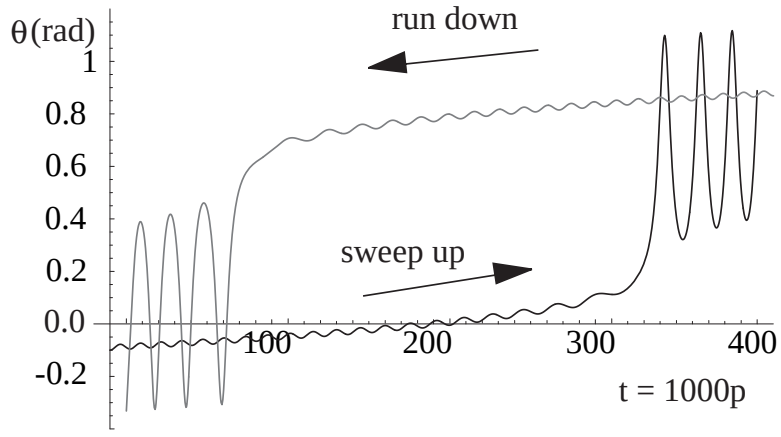

Evolution through snap-through illustrating hysteresis. Initial conditions: For both $\dot{\theta} = 0.0$, $\theta(0) = -0.1$ *at* $t = 0$ *and* $\theta(0) = 0.8654$ *at* $t = 400$

We note finally that, unlike for symmetric systems possessing a trivial equilibrium solution, this type of limit point buckling is not sensitive to initial imperfections.

The local stiffness of the force-deflection curve can be obtained from the derivative of the equilibrium condition, i.e.,

$$\frac{dp}{d\theta} = \frac{\cos\alpha - \cos^3(\alpha - \theta)}{\cos^2(\alpha - \theta)}, \tag{68}$$

which in turn can be related to the effective linear natural frequency in the usual way.

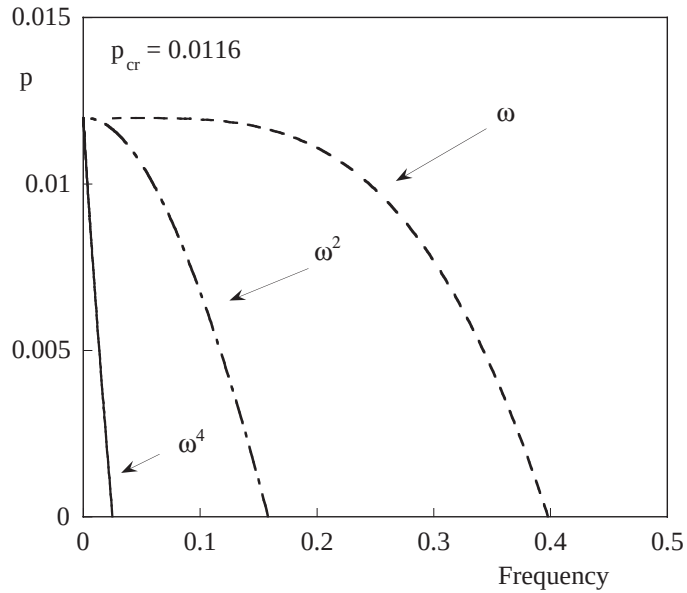

The relation between the natural frequency and load for the snap-through model.